Theoretical and Experimental Analysis on Influence of Revolution Radius in Orbital Drilling

Yang Yinfei(杨吟飞)[1*], *Shan Yicai*(单以才)[1,2], *Zhang Ting*(章婷)[3], *He Ning*(何宁)[1], *Li Liang*(李亮)[1]

1. College of Mechanical and Electrical Engineering, Nanjing University of Aeronautics and Astronautics, Nanjing, 210016, P. R. China;
2. Department of Mechanical and Engineering, Nanjing College of Information Technology, Nanjing, 210023, P. R. China;
3. School of Mechanical Engineering, Nanjing Institute of Technology, Nanjing, 211167, P. R. China

(Received 10 September 2013; revised 27 April 2014; accepted 8 May 2014)

Abstract: Revolution radius is one of the significant parameters in orbital drilling, which has great influence on many factors, such as the cutting area of front and side cutting edge, undeformed chip geometry, delamination and burr at hole exit side, hole surface roughness, cutting tool force and deflection, chip removal and heat transmission. First, the influence of revolution radius on the factors is discussed theoretically in detail. Analysis results show that big revolution radius can reduce axial cutting force, restrain exit delamination and burr, and improve chip removal and heat transmission. Then, single factor test and orthogonal test are utilized in the two processing methods as machining unidiameter holes with several cutting tools and machining different diameter holes with one tool. Finally, the influence of revolution radius on cutting force and hole machining precision is studied. These results provide a profound foundation for future optimization of cutting control parameters.

Key words: robotic hole-making system; orbital drilling; revolution radius; milling forces; hole quality

CLC number: TG506.1 **Document code**: A **Article ID**: 1005-1120(2014)05-0498-10

1 Introduction

With successful production of domestic regional airplane ARJ-700 and in-depth research on big plane C919, robotic hole-making technology has been a research hotspot in plane final assembly[1-5]. However, present robotic hole-making systems are usually equipped with end effector for drilling, which is only suitable for machining small holes. To meet the demands of high efficiency and precision in processing large-deep hole with aerospace hard-cutting materials, the development of new end effector and hole-making technology is urgent in China[6-8].

Orbital drilling is a new hole-making technology with compound milling[9]. During orbital drilling, the cutting tool orbits round the center of the hole while rotating on its own axis and moving in the axial direction. The revolution movement of the cutting tool can complete one-time hole processing. Different revolution radius helps to process different diameter holes with one tool. Moreover, revolution movement contributes to lowering burr formation in metal, reducing delamination in carbon fiber reinforced plastics (CFRP), decreasing axial cutting force and improving the ability of chip removal[10-11]. Therefore, intensive research of orbital drilling technology is worth considering.

Besides the rotation movement of the cutting tool and axial feed as drilling, the revolution movement of the cutting tool is added in orbital drilling. Compared with conventional drilling, the movement in orbital drilling is more difficult to be controlled. Denkena, et al. analyzed the impact of axial and tangential feed on milling

Foundation item: Supported by the Major Science and Technology Project (2012ZX04003-031).

* **Corresponding author**: Yang Yinfei, Lecturer, E-mail: yyfgoat@nuaa.edu.cn.

forces through undeformed chip model[12]. Shigemoto Aakamot, et al. studied the influence of revolution speed on cutting temperature when machining CFRP, and found that the increase of revolution speed might lower cutting temperature[13]. Shan, et al. utilized the function of orbital drilling on horizontal lathe to study the feasibility of orbital drilling with big pitch[14]. As an important control parameter in orbital drilling, the variation of the revolution radius has a great effect on many factors including working efficiency, hole quality and tool wear, etc. However, few researches focus on the effects. We attempt to study the influence of revolution radius on milling force and hole quality.

2 Theoretical Analysis of Revolution Radius Affecting Orbital Drilling Movement

2.1 Effects of revolution radius on two cutting zones

Fig. 1 shows the principle of orbital drilling[9]. In orbital drilling, the front and the side cutting edges involve in processing simultaneously. When analyzing the movement of the cutting

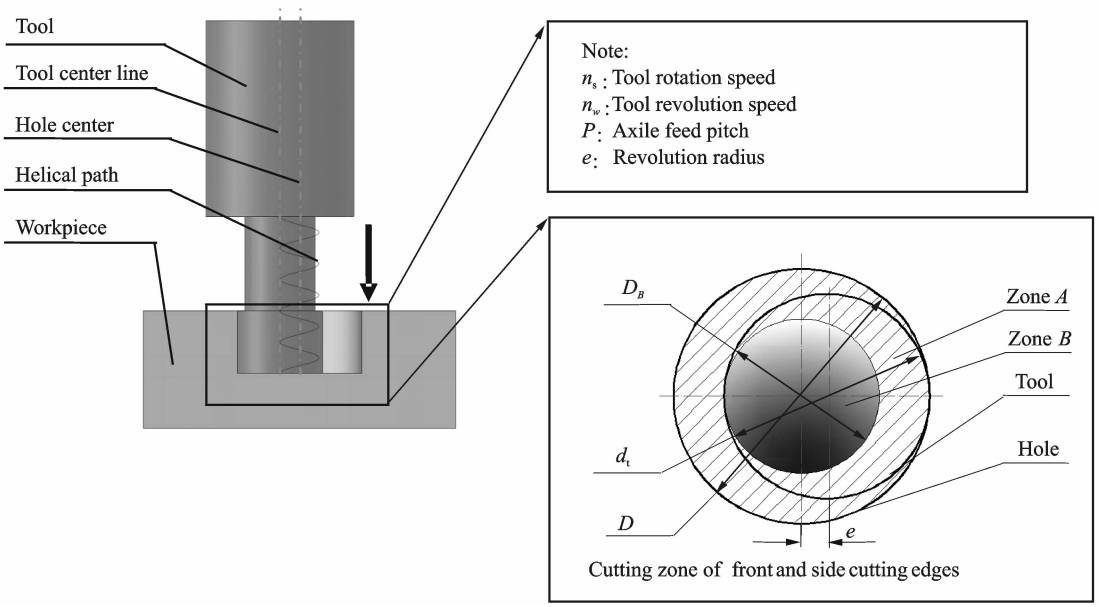

Fig. 1 Orbital drilling

tool related to the workpiece, we know the front cutting edge conducted continuous milling, while the side cutting edge performs discontinuous milling. The two milling motions lead to the differences in cutting force distribution and chip shape at two cutting zones.

The graphic in the bottom right corner of Fig. 1 gives the distribution of two cutting zones. Here, zone B refers to the region of the smallest circle. The material in zone B is only removed by front cutting edge. Zone A represents the shadow area outside of zone B where front and side cutting edge both participate in processing. D_B is the diameter of zone B.

R_B, the radius of zone B is calculated as

$$\begin{cases} e=(D-d_t)/2 \\ R_B=d_t/2-e \end{cases} \tag{1}$$

where D is the diameter of the hole, d_t the diameter of the cutting tool. When $R_B=d_t/2$ and $e=0$, the machining method is conventional drilling. When $R_B=d_t/2-e$ and $e\neq 0$, orbital drilling can be realized.

In zone B, the axial feed per tooth of front cutting edge is a constant value, which is calculated as

$$f_{B,z}=(P\times n_w)/(n_s\times Z) \tag{2}$$

where Z is the number of tool tooth.

In zone A, the axial cutting depth of side

cutting edge and the axial feed per tooth of front cutting edge both change with the radial position of the hole. The axial cutting depth of side cutting edge is calculated as Eq. (3), while the axial feed per tooth of front cutting edge can be expressed by Eq. (4)

$$f^*_{T,z} = P * \arccos[(x * x + e * e - (d_t/2) * (d_t/2))/(2 * x * e)]/\pi \quad (3)$$

$$f^*_{B,z} = P - f^*_{T,z} \quad (4)$$

where $R_B \leqslant x \leqslant D/2$. Fig. 2 shows the distribution of axial cutting depth and axial feed along the radial direction of the hole.

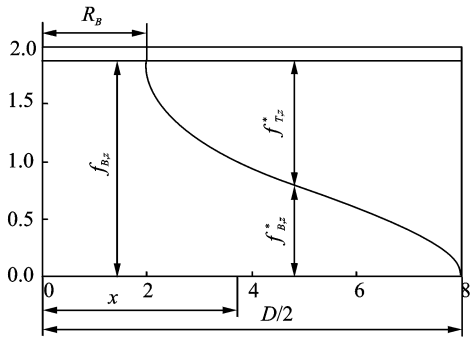

Fig. 2 Distribution of axial cutting depth and axial feed along radial direction of hole

When e increases, the area of zone B reduces and the cutting area of front cutting edge decreases. While in zone A, the cutting area of the two cutting edges increases, which helps to decrease axial cutting force.

2.2 Effect of revolution radius on undeformed chip geometry

According to Ref. [12], the undeformed chip model in orbital drilling is established as shown in Fig. 3. Eq. (5) shows the maximum tangential feed per tooth and the axile cutting depth of the side cutting edge. Eq. (6) gives the maximum axial feed per tooth and the radial cutting width of the front cutting edge

$$\begin{cases} f_{zt,\max} = 2\pi \times e \times n_w/(n_s \times Z) \\ a_P = f^*_{T,z} \end{cases} \quad (5)$$

$$\begin{cases} f_{za,\max} = P \times n_w/(n_s \times Z) \\ a_e = d_t/2 \end{cases} \quad (6)$$

where $f_{zt,\max}$ is the maximum tangential feed per tooth of the side cutting edge. $f_{za,\max}$ the maximum axial feed per tooth of the front cutting edge. The two parameters are both related to geometrical parameter, rotation speed, revolution speed and revolution radius.

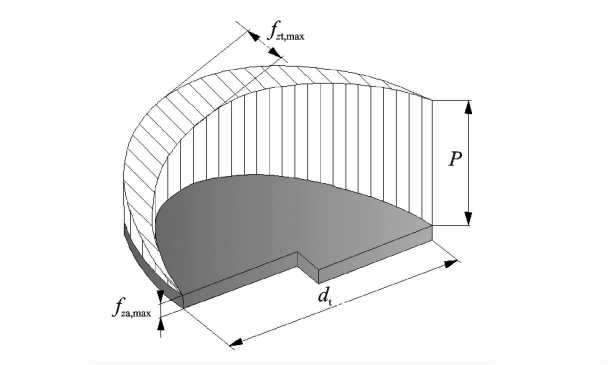

Fig. 3 Undeformed chip geometry during orbital drilling

As for a special hole, the increase of e with unchanging the other cutting condition, brings about the increase of $f_{zt,\max}$ and the decrease of d_t while $f_{za,\max}$ and a_p remains unchanged. Therefore, for the side cutting edge, the tangential cutting thickness per tooth becomes larger, and its axial cutting depth remain unchanged. For the front cutting edge, the axial feed per tooth remains unchanged, but its radial cutting width becomes smaller. These above-mentioned changes of undeformed chip geometry have directly impact on milling force and chip removal.

2.3 Effect of revolution radius on delamination and burr at exit side

In conventional drilling, metal burrs and CFRP delamination are two major defects. In industrial manufacturing of closed structures, the drilling process is composed of several steps as assembling, hole-making, disassembling, deburring and reassembling, which greatly affects the machining efficiency.

Fig. 4 gives the schematic of hole-making in CFRP. We simplify the material at hole bottom as a beam model, which is under the cutting force. During conventional drilling as shown in Fig. 4(a), the material at hole bottom is squeezed and further separated from workpiece by the axial cutting force. The axial cutting force acts upon the middle of the beam model. With the existence

of revolution radius of orbital drilling, the axial cutting force gets smaller and acts on the position deviated from the middle. When comparing the two machining methods, we find that the delamination at the hole exit side in Fig. 4(b) is much smaller than that in Fig. 4(a). Therefore, orbital drilling contributes to the decrease of CFRP delamination.

Fig. 5 shows burr and formation at the hole exit side while machining aluminum alloy 2024 workpiece[15]. Since the material at the hole exit is squeezed by axial thrust force from chisel edge, a large number of burr piles up at the orifice as shown in Fig. 5(a). The other two pictures of Fig. 5 reveal two caps under two different values of e/D_H in orbital drilling. Seen from Figs. 5(b, c), there is little burr appearing at the hole edge. The reason is that the material at the hole exit is removed by side cutting edge. Meanwhile, when e/D_H increases, the cap becomes smaller.

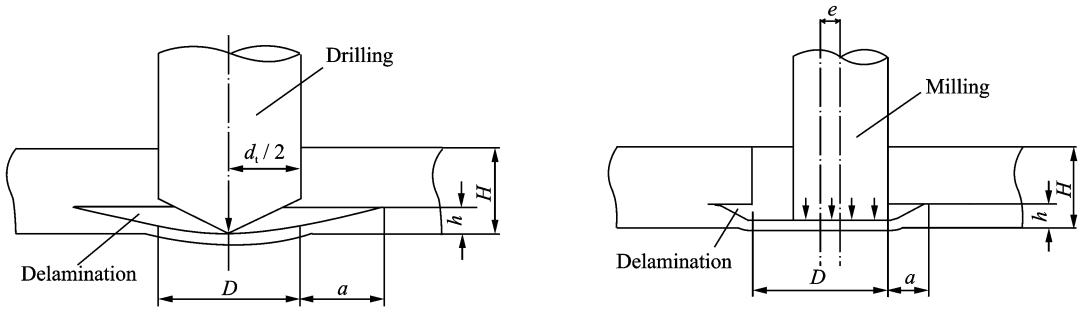

(a) Conventional drilling (b) Orbital drilling

Fig. 4 Effect of revolution radius on delamination at hole exit side

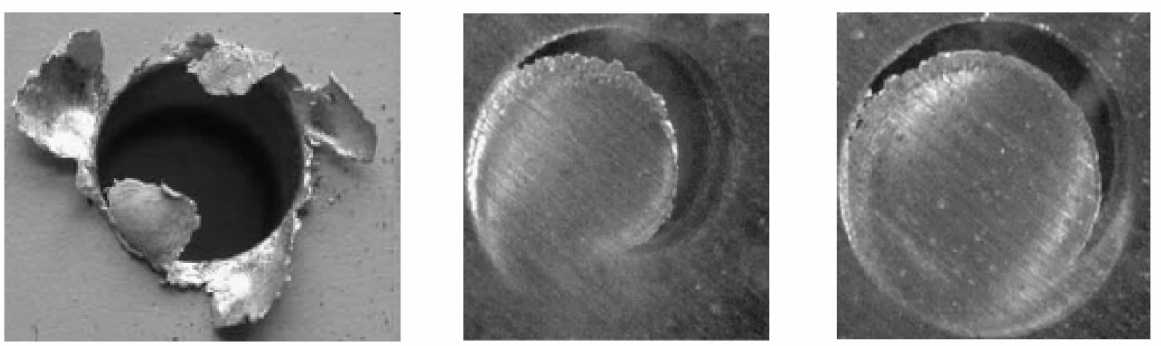

(a) Conventional drilling (b) Orbital drilling when e/D_H=0.155 (c) Orbital drilling when e/D_H=0.108

Fig. 5 Effect of revolution radius on burr and formation at hole exit side

2.4 Effect of revolution radius on hole surface roughness

Since surface roughness is a key index of hole quality, the influence of revolution radius on hole surface roughness is analyzed theoretically in the following.

Fig. 6 gives a theoretical model for calculating hole surface roughness. When tool rotates one tooth, the tool revolution angle is φ_ω, namely

$$\varphi_\omega = \frac{2\pi n_\omega}{Z n_s} = \frac{2\pi}{Z\lambda} \tag{7}$$

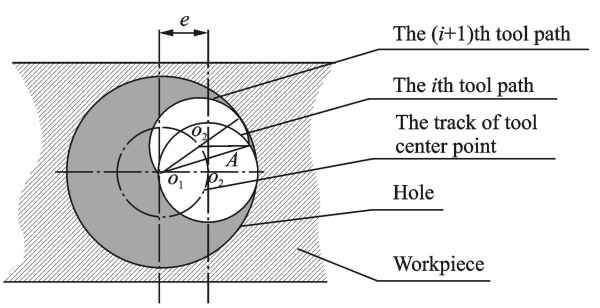

Fig. 6 Theoretical calculation model of hole surface roughness

where λ is the speed ratio of cutting tool n_s and n_w.

From Fig. 6, hole surface roughness R_z is expressed as

$$R_z = D/2 - l_{O_1A} = e + d_t/2 - l_{O_1A} \tag{8}$$

where l_{O_1A} means the distance from point O_1 to point A, which can be expressed as

$$l_{O_1A} = \frac{d_t}{2} \times \sin(\pi - \varphi_\omega/2 - \arcsin(e\sin(\varphi_\omega/2)/(d_t/2)))/\sin(\varphi_\omega/2) \tag{9}$$

When substituting Eqs. (7, 9) into Eq. (8), we gain

$$R_z = e + \frac{d_t}{2} \cdot \{1 - \sin(\pi - \pi/(Z\lambda) - \arcsin((e\sin(\pi/(Z\lambda)))/(d_t/2)))/(\sin(\pi/Z\lambda))\} \tag{10a}$$

or

$$R_z = \frac{D}{2} - (\frac{D}{2} - e)\left\{\sin(\pi - \frac{\pi}{Z\lambda} - \arcsin(e\sin(\frac{\pi}{Z\lambda})/(\frac{D}{2} - e)))/\sin(\frac{\pi}{Z\lambda})\right\} \tag{10b}$$

Eq. (10) is a theoretical formula of surface roughness in orbital drilling.

When d_t is set as 12 mm and Z as 2, the relations of three parameters as R_z, e and λ are shown in Fig. 7. With the variation of e, D changes accordingly. Under different values of e, the tendency of all curves are almost the same. With the increase of e, the value of R_z increases gradually. When λ is small, small increment of e leads to big increment of R_z. When λ is big, the change of R_z becomes slowly. Fig. 7 also indicates that the influence of e on R_z is smaller than that of λ. Fig. 8 reflects the effect of e and λ on R_z when using different tools with two teeth to machine 23 mm hole. To machine a hole with specific diameter, we can set different revolution radiuses to meet the demand of different tools. The change of curves in Fig. 8 is very similar to the tendency in Fig. 7. That is, (1) When e is gradually increasing, R_z slightly increases. (2) When λ is decreasing, R_z greatly increases.

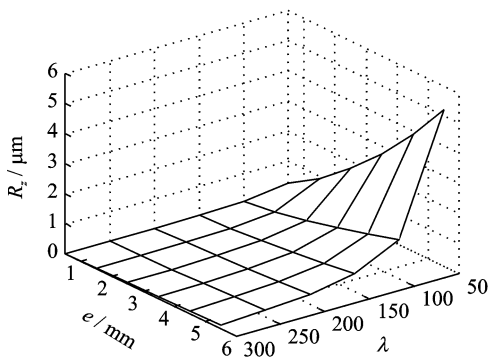

Fig. 7 Relationship of R_z with e, λ when $d_t = 12$ mm, $Z = 2$

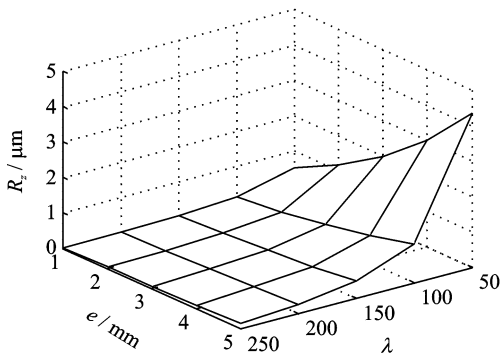

Fig. 8 Relationship of R_z with e, λ when $D = 23$ mm, $Z = 2$

2.5 Effect of revolution radius on chip removal and cutting heat dissipation

In orbital drilling, hole diameter is larger than cutting tool diameter. Therefore, a crescent gap appears between the cutting tool and the hole surface. The small chip produced by side cutting edge is mainly removed through the crescent gap. And the long chip produced by front cutting edge is removed through the helix channels of the cutting tool. Obviously, the two kinds of chip have different chip removal channels and the two chip removal methods are independent from each other.

The cutting heat dissipation mode in orbital drilling is different from that in drilling. The heat transmitted to the cutting tool and the work-piece is greatly reduced by the discontinuous milling of side cutting edge. As there is a crescent gap in orbital drilling, the cutting heat dissipation mode shows three ways as conduction, convection and radiation[16]. Under low rotation speed and small revolution radius, air flow between cutting tool and hole surface is stable and similar to laminar

flow. The heat dissipation mainly depends on convection. With the increase of rotation speed and revolution radius, the air flow becomes unstable. Then, heat conduction becomes significant.

3 Experimental Design

3.1 Experimental setup

Orbital drilling experiment is conducted on high speed machining center of Mikron UCP710, as shown in Fig. 9. The workpiece material is aluminum alloy 6061. The cutting tools from German Walter company are H602411-8, H602411-10 and H602411-12, which have 45° helix angle and two teeth. To avoid the influence of tool clamping length on hole machining accuracy, the three cutting tools are installed with the same overhanged length. Dry cutting and upmilling are adopted in the experiment. Milling force measurement system is composed of Kistler 9265B dynamic force measurement instrument, Kistler 5019 charge amplifier, and computer data acquisition system. When cutting force signal is stable, we select 100 adjacent peaks and troughs. From each four adjacent peaks and troughs, we chose the highest peak and the lowest trough. Then two average values of the 25 peaks and troughs are calculated respectively. The bigger absolute average value is regarded as measured value of cutting force. Surface roughness is measured by surface roughness tester Mahr M1. Average value of three measurements at three positions is regarded as the value of hole surface roughness.

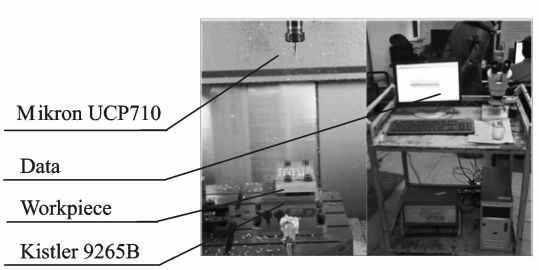

Fig. 9 Experimental setup

3.2 Cutting control parameters

With the revolution radius, orbital drilling can realize the functions of machining one hole by different cutting tools and machining different holes by one cutting tool. To study the influence of revolution radius on milling forces and hole surface roughness, the single-factor experiments are carried out by machining the same holes with different cutting tools. When tool rotation speed, revolution speed, and axial feed pitch are all set as constant values, a hole of φ 14 mm is processed in Al6061 through cutting tools H602411-8, H602411-10 and H602411-12. Cutting control parameters of orbital drilling are designed in Table 1.

Table 1 Cutting control parameters of orbital drilling

No.	n_s/(r·min^{-1})	n_w/(r·min^{-1})	P/mm	e/mm	d_t/mm
1	4 000	23.87	1	3	8
2	4 000	23.87	1	2	10
3	4 000	23.87	1	1	12
4	6 000	31.82	1	3	8
5	6 000	31.82	1	2	10
6	6 000	31.82	1	1	12

To discuss the process ability when machining different holes by one cutting tool, the influence of revolution radius on milling forces and hole surface roughness is further studied on the basis of orthogonal tests with H602411-10. Table 2 gives the values of cutting controlling parameters, hole surface roughness R_z, axile cutting force F_a and radial cutting force F_r.

Table 2 Cutting control parameters and values of R_z and F_a/F_r

No.	n_s/(r·min^{-1})	n_w/(r·min^{-1})	P/mm	e/mm	d_t/mm	F_a/N	F_r/N	R_z/μm
1	3 000	15.92	1	1	10	59.27	51.16	0.35
2	3 000	31.82	1	1	10	100.92	56.05	0.32
3	3 000	23.87	2	2	10	119.34	124.51	0.39
4	3 000	31.82	2	2	10	145.07	134.43	0.47
5	4 000	15.92	2	1	10	107.96	56.81	0.33
6	4 000	31.82	2	1	10	144.18	77.62	0.38

Continued

No.	n_s/(r·min^{-1})	n_w/(r·min^{-1})	P/mm	e/mm	d_t/mm	F_a/N	F_r/N	R_z/μm
7	4 000	23.87	1	2	10	107.58	81.32	0.41
8	4 000	31.82	1	2	10	112.82	85.96	0.48
9	5 000	15.92	1	1	10	78.51	55.55	0.36
10	5 000	31.82	1	1	10	95.57	63.38	0.37
11	5 000	23.87	2	2	10	119.23	174.40	0.45
12	5 000	31.82	2	2	10	140.82	206.85	0.50
13	6 000	15.92	2	1	10	89.38	38.77	0.36
14	6 000	31.82	2	1	10	108.81	57.12	0.31
15	6 000	15.92	1	2	10	97.41	53.20	0.39
16	6 000	31.82	1	2	10	92.29	60.60	0.34

4 Experimental Results and Analysis

4.1 Effect of revolution radius when machining unidiameter holes by different cutting tools

4.1.1 Milling forces

Fig. 10 shows the influence of revolution radius on axile and radial cutting force. With the increase of e, F_a obviously decreases, while F_r changes little. Under different revolution radius, the curves of F_r present the same trend.

Combined with Fig. 1, we can give the following explanation for the curves in Fig. 10: The increase of e increases the cutting zones of side cutting edge, while decreases that of front cutting edge. According to Eqs. (5,6), when tool rotation speed, revolution speed and axial feed pitch all remain unchanged, the increase of revolution radius makes the axial cutting depth of side cutting edge remain unchanged, while its tangential cutting thickness becomes big. As for front cutting edge, the axial cutting depth remains unchanged with the increase of e, while the radial cutting width becomes small. Therefore, the sharp decline of F_a is mainly caused by the increase of e. However, F_r always changes little, which is caused by the little influence of tangential cutting thickness.

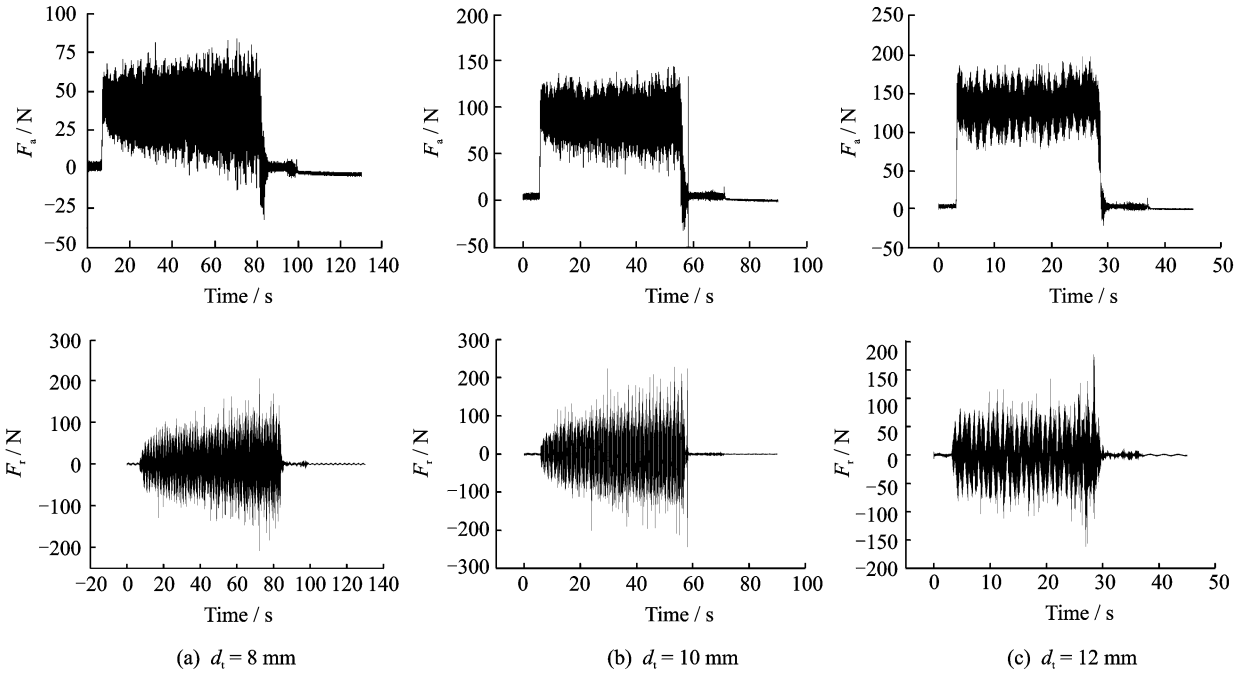

Fig. 10 Effect of revolution radius on milling forces when n_s = 4 000 r/min, n_w = 23.82 r/min; a_p = 1 mm

4.1.2 Hole machining precision

After a hole of φ = 14 mm is processed respectively by H602411-8, H602411-10 and H602411-12, the true size of hole diameter is measured as shown in Fig. 11. When n_s is 4 000 r/min, n_w is 23.87 r/min, and P is 1 mm, the best dimensional accuracy of hole is achieved by H602411-10, the second-best dimensional accuracy is by H602411-8, and H602411-12 makes the worst accuracy. The cutting tool rigidity and axi-

al cutting force from big to small are both H602411-12, H602411-10 and H602411-8. The hole diameter error depends on the comprehensive effect of cutting tool rigidity and force. When n_s=6 000 r/min, n_w = 31.82 r/min, and P = 1 mm, H602411-8 gains the best dimension accuracy, while H602411-12 leads to the worst accuracy. The experimental result shows small diameter cutting tool is always under small axial cutting force, the increase of cutting control parameter can reduce aperture error.

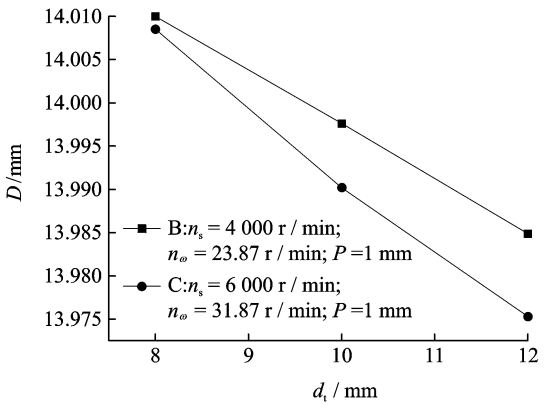

Fig. 11 Effect of revolution radius on hole diameter

4.2 Effect of revolution radius when machining different holes by one cutting tool

4.2.1 Significant analysis on the effect of revolution radius

In Table 2, t-state is the t-statistic of coefficient of interest. P-value denotes the probability which is equal to or greater than statistic observation values when taking a random sampling from overall samples. Hole surface roughness lies between 0.3 and 0.5 μm, which belongs to high-precision machining. Through orbital drilling, high precision hole can be machined in once time, which improves the processing efficiency greatly.

With the input of Table 2, quadractic regression analysis is conducted on R_z and F_r/F_a. Analysis result is shown in Table 3. As for R_z, the biggest absolute t value of e indicates that e has the largest impact on R_z. The reason is the variation of e determines the changes of cutting zone area and crescent gap which directly effect on R_z. When analyzing F_a, e has the third effect on F_a after P and n_w. The absolute t value 3.25 shows e is the biggest impact factor on F_r.

Table 3 Analysis of variance for R_z and F_r/F_a

Parameter		Coefficient	Standard error	t-state	P-value
F_a	n_s	−0.002 83	0.002 68	−1.05	0.315
	n_w	1.475 90	0.044 02	3.35	0.006
	P	27.366 00	6.000 10	4.56	0.001
	e	14.345 00	6.127 00	2.34	0.039
F_r	n_s	−0.006 08	0.007 38	−0.82	0.427
	n_w	1.163 00	1.207 00	0.96	0.356
	P	44.260 00	16.460 00	2.69	0.021
	e	54.630 00	16.81	3.25	0.008
R_z	n_s	-1.2×10^{-5}	0.000 0	−0.91	0.483
	n_w	-6.3×10^{-5}	0.002 3	−0.03	0.649
	P	2.5×10^{-3}	0.029 3	0.09	0.380
	e	7.025×10^{-2}	0.030 8	2.28	0.005

4.2.2 Interaction influence of revolution radius and other parameters

Fig. 12 shows response faces of revolution radius with other cutting control parameters on milling forces. Figs. 12(a,b) show that, with the increase of n_s, F_a/F_r first increases then decreases; Under a specified n_s, F_a/F_r varies monotonically with the variation of e. Moreover, the variation of F_a is relatively obvious while F_r changes slowly.

In Fig. 12(c), the increase of e and n_w might improve the value of F_a. The effect of e on F_a is smaller than that of n_w. The influence of e and n_w on F_r is very complicated which can be seen from Fig. 12(d). In the stage of low n_w, F_r shows a downward trend with the increase of e. While under high n_w, F_r presents the opposite trend.

Compared with Figs. 12(c, e), the two graphics have the same variation tendency. With P increasing, F_a increases significantly. When P is bigger, the variation of e has little influence on F_a. With small P, the increase of e can obviously increase F_a. Known from Fig. 12(f), the influence of e and P on F_r is very complex. When e is small, F_r decreases with P increaseing. While e becomes bigger, F_r significantly increases with P.

Fig. 13 is response faces of e with other cut ting control parameters on R_z . It can be seen

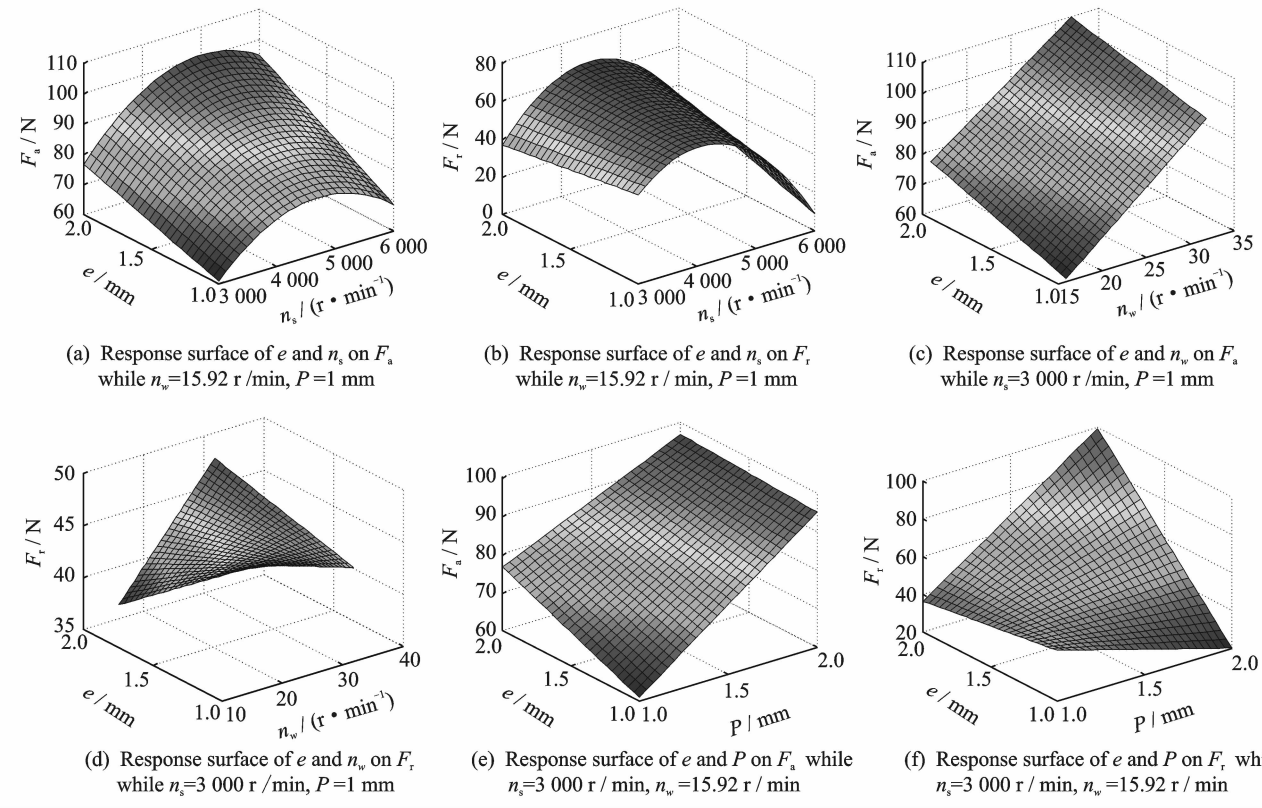

(a) Response surface of e and n_s on F_a while n_w=15.92 r /min, P=1 mm

(b) Response surface of e and n_s on F_r while n_w=15.92 r / min, P=1 mm

(c) Response surface of e and n_w on F_a while n_s=3 000 r /min, P=1 mm

(d) Response surface of e and n_w on F_r while n_s=3 000 r /min, P=1 mm

(e) Response surface of e and P on F_a while n_s=3 000 r / min, n_w=15.92 r / min

(f) Response surface of e and P on F_r while n_s=3 000 r / min, n_w=15.92 r / min

Fig. 12 Response surface of interaction between e and other parameters on F_a and F_r

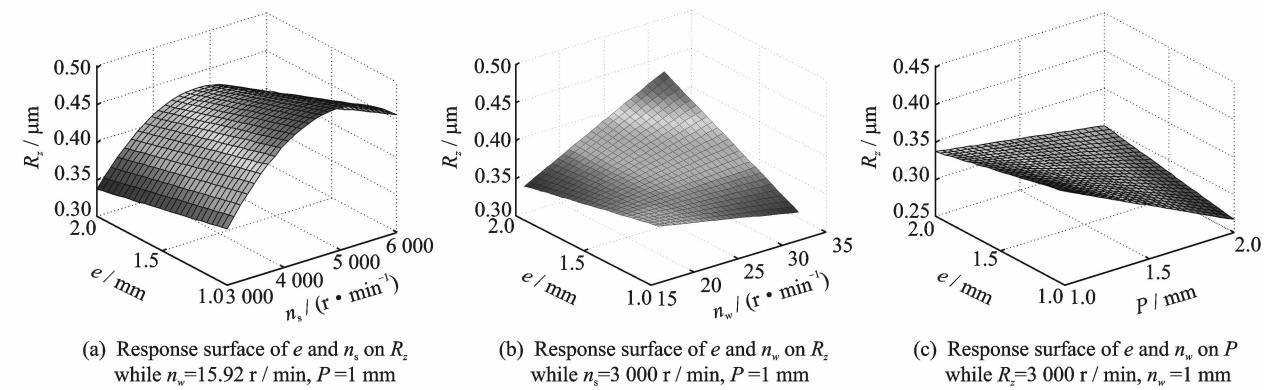

(a) Response surface of e and n_s on R_z while n_w=15.92 r / min, P=1 mm

(b) Response surface of e and n_w on R_z while n_s=3 000 r / min, P=1 mm

(c) Response surface of e and n_w on P while R_z=3 000 r / min, n_w=1 mm

Fig. 13 Response surface of interaction between e and other parameters on R_z

from Fig. 13(a) that with the increase of n_s, R_z firstly increases, and then gradually reduces. Subjected by a combination of various factors as cutting force and chip removal, etc. R_z decreases with the increase of e when n_s is set at constant value.

Fig. 13(b) presents a complicated influence of e and n_w on R_z. When e increases, R_z slightly decreases at low n_w and obviously increases at high n_w. In Fig. 13(c), R_z shows a linear change with e and P. When e increases, R_z slightly decreases at small P, and obviously increase at big P.

5 Conclusions

(1) Theoretical analysis indicates the cutting zone of front cutting edge decreases with the increase of e, while the cutting zone of side cutting edge enlarges. As for undeformed chip geometry, the cutting thickness per tooth of side cutting edge increases, while radial cutting width of front cutting edge decreases. When machining CFRP and metal, small values of F_a and e help to re-

strain delamination and burr at hole exit side. The increase of crescent gap is helpful for chip removal and heat transmission.

(2) Single factor test shows F_a increases following the decrease of e when machining the hole with one diameter, while F_r almost remains unchanged. Constrained by cutting tool rigidity, cutting force and centrifugal force, hole maching precision achieved by three cutting tools are different from each other. The order of hole machining precision from high to low is H602411-10, H602411-8 and H602411-12 at low n_s. While at high n_s, the order changes to H602411-8, H602411-10 and H602411-12.

(3) Orthogonal tests indicate the influence of e on R_z is more significant than that on F_a/F_r. The united influence of e and other parameters on R_z are detailedly studied under different cutting conditions. The analysis result provides scientific guidance for cutting control parameters optimization during orbital drilling by a single cutting tool.

References:

[1] Devlieg R, Sitton K, Feikert E, et al. ONCE (one sided cell end effector) robotic drilling system[C]// 2002 SAE Automated Fastening Conference & Exhibition. USA:SAE,2002:2002-01-2626.

[2] Atkinson J, Hartmann J, Jones S, et al. Robotic drilling system for 737 aileron[C]// Aerospace Technology Conference and Exhibition. USA: SAE, 2007:2007-01-3821.

[3] Bi Shusheng, Liang Jie. Robotic drilling system for titanium structures[J]. Int J Adv Manuf Technol, 2011,54(5-8):767-774.

[4] ShanYicai, He Ning, Li Liang. Vector modeling of robotic helical milling hole movement and theoretical analysis on roughness of hole surface[J]. Journal of Central South University of Technology, 2013, 20(7):1818-1824.

[5] Du Baorui, Feng Ziming, Yao Yanbin. Robot drilling system for automatic drilling of aircraft component [J]. Aeronautical Manufacturing Technology, 2010(2):47-50. (in Chinese)

[6] WangJian, Liu Hao, Tian Wei, et al. Design of drilling end effector for aircraft automatic assembly [J]. Journal of Nanjing University of Aeronautics & Astronautics, 2012,44(S1):19-22. (in Chinese)

[7] He Ning, Li Liang, Shan Yicai, et al. Automatic wing-body docking hole-making system and method: China,2L201010138456.6[P]. 2010-3-1[2013-9-10], 2010,3.

[8] Liang Jie, Bi Shusheng. Design and experimental study of an end-effector for robotic drilling[J]. Int J Adv Manuf Technol,2010,50(1-4):399-407.

[9] Brinkmeier E, Fangmann S, Meyer I. Orbital drilling kinematics[J]. Production Engineering (WGP), 2008, 2(1): 277-283.

[10] Iyer R, Koshy P, Ng E. Helical milling: An enabling technology for hard machining precision holes in AISI D2 tool steel[J]. International Journal of Machine Tool & Manufacture,2007,47(2): 205-210.

[11] Ni Wangyang. Orbital drilling of aerospace materials [C]// SAE 2007 Transactions Set. Los Angeles: SAE International, 2008,116: 2007-01-3814.

[12] Denkena B, Boehnke D, Dege J H. Helical milling of CFRP-titanium layer compounds [J]. CIRP Journal of Manufacturing Science and Technology, 2008, 2(1): 64-69.

[13] Shigemoto Aakamot, Hirkoki Iwasa. Effect of cutting revolution speed on cutting temperature in helical milling of CFRP composite laminates [J]. Key Engineering Materials, 2012,523-524: 58-63.

[14] Shan Yicai, He Ning, Li Liang, et al. Orbital milling hole of aerospace Al-alloy with big pitch [J]. Transactions of Tianjin University, 2011,17(5):229-235.

[15] Brinksmeier E, Fangmann S. Burr and cap formation by orbital drilling of aluminum[J]. Annals of the CIRP, 1996, 46(1): 401-404.

[16] Sadek A, Meshreki M, Attia M H. Characterization and optimization of orbital drilling of woven carbon fiber reinforced epoxy laminates [J]. CIRP Annals Manufacturing Technology, 2012,61(1):123-126.

(Executive editor: Zhang Bei)